Impact of Increased Sonication-Induced Dispersion of Sepiolite on Its Interaction with Biological Macromolecules and Toxicity/Proliferation in Human Cells

David Adame Brooks, Olivier Piétrement, Elodie Dardillac, Ayesha Jayantha, Manuel Lores Guevara, Fidel Antonio Castro-Smirnov, Pilar Aranda, Eduardo Ruiz-Hitzky, Bernard Lopez

ACS OMEGA

http://pubs.acs.org/journal/acsodf

Article

Impact of Increased Sonication-Induced Dispersion of Sepiolite on Its Interaction with Biological Macromolecules and Toxicity/Proliferation in Human Cells

David Adame Brooks, Olivier Piétrement, Elodie Dardillac, Ayesha Jayantha, Manuel A. Lores Guevara, Fidel Antonio Castro-Smirnov, Pilar Aranda, Eduardo Ruiz-Hitzky, and Bernard S. Lopez*

Cite This: *ACS Omega* 2023, 8, 1026−1036

Read Online

ACCESS | Metrics & More | Article Recommendations

ABSTRACT: Sepiolite is a natural clay silicate that is widely used, including biomedical applications; notably sepiolite shows promising features for the transfer of biological macromolecules into mammalian cells. However, before its use, such an approach should address the efficiency of binding to biological macromolecules and cell toxicity. Because sepiolite spontaneously forms aggregates, its disaggregation can represent an important challenge for improving the suspension performance and the assembly with biological species. However, this can also influence the toxicity of sepiolite in mammalian cells. Here, a very pure commercial sepiolite (Pangel S9), which is present as a partially defibrillated clay mineral, is used to study the consequences of additional deagglomeration/dispersion through sonication. We analyzed the impact of extra sonication on the dispersion of sepiolite aggregates. Factors such as sonication time, sonicator power, and temperature are taken into account. With increasing sonication time, a decrease in aggregation is observed, as well as a decrease in the length of the nanofibers monitored by atomic force microscopy. Changes in the temperature and pH of the solution are also observed during the sonication process. Moreover, although the adsorption capacity of bovine serum albumin (BSA) protein on sepiolite is increased with sonication time, the DNA adsorption efficiency remains unaffected. Finally, sonication of sepiolite decreases the hemolytic activity in blood cells and the toxicity in two different human cell lines. These data show that extra sonication of deagglomerated sepiolite can further favor its interaction with some biomacromolecules (e.g., BSA), and, in parallel, decrease sepiolite toxicity in mammalian cells. Therefore, sonication represents an alluring procedure for future biomedical applications of sepiolite, even when using commercial defibrillated particles.

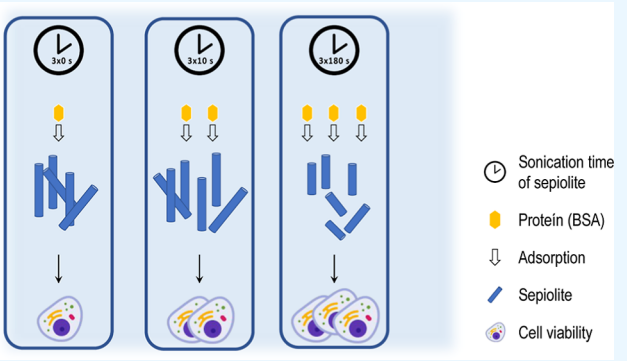

1. INTRODUCTION

Sepiolite and palygorskite belong to a clay mineral family of silicates of fibrous morphology with interesting crystal structures and surface properties as they show a large specific surface area and the presence of silanol groups (≡Si−OH), facilitating the interaction with diverse types of compounds. Due to these characteristics, sepiolite is mainly used for its adsorbent and rheological properties.[1,2] These clay minerals are marketed for a wide variety of uses and are nowadays intensively investigated for the development of numerous advanced materials.[3−21] In the last decade, sepiolite has attracted growing interest for biomedical applications. Indeed, sepiolite has been shown to be able to bind different kinds of biological macromolecules, including polysaccharides, lipids, proteins, and DNAs.[20−24]

Sepiolite is a hydrated magnesium silicate with a unit cell formula of $Si_{12}O_{30}Mg_8(OH, F)_4(OH2)_4{\cdot}8H_2O$; its structural arrangement consists of alternate magnesium silicate blocks and intracrystalline cavities named tunnels that grow in the crystallographic *c*-direction. Tunnels that reach the external surface of sepiolite fibers can be considered as channels. These structures are involved in the interaction between the silicate and many diverse compounds, in particular through silanol groups (≡Si−OH) located at the edges of the channels.[25,26]

Other active sites at the sepiolite interface include the negatively charged surface attributed to isomorphical substitution of Mg^{2+} ions by Al^{3+} ions and other trivalent cations in the octahedral layers. These two types of active sites are

Received: October 3, 2022
Accepted: December 15, 2022
Published: December 28, 2022

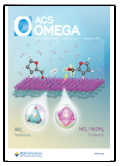

central to the adsorption mechanisms that occur at the external surfaces of fibrous clay minerals.[26]

Natural raw sepiolite appears at the electronic microscope as bundles resulting from the agglomeration of their silicate microfibers, which can be disaggregated in concentrated water dispersions by applying high-speed mechanical shearing or by ultrasonication. The resulting products at the industrial level are considered samples of "rheological grade" sepiolite products, which have been commercialized as thickening or suspending agents (e.g., Pangel S9).[27,28] However, such materials still contain aggregates, and it has been shown that their further dispersion can improve efficacy regarding many different applications. For instance, detangled sepiolite promotes the transfer of DNA into mammalian cells, but the efficiency can be optimized through additional sonication of sepiolite (sSep) before the synthesis of the bionanocomposite sSep/DNA.[20]

Therefore, for the use of sepiolite in different applications, increased disaggregation can be important for wider spreading and the formation of stable and homogeneous suspensions that are crucial steps to improve their performance. Some mechanical irradiation (ultrasounds) has also been proposed as a procedure to efficiently defibrillate sepiolite to generate colloidal routes to obtain new heterostructured functional nanomaterials.[26]

The individual particles of sepiolite (even those that have been previously defibrillated) can easily aggregate in water through hydrogen bonding and van der Waals interactions to form bundles and aggregates, limiting clay dispersion.[29] Of note, a recent study reports on the colloidal dispersion behavior of individual sepiolite fibers by analyzing the diffusive motion of some natural clays. The authors show that sepiolite nanoclay demonstrates rich Brownian-type rotational dynamics.[30] To improve the dispersibility of sepiolite, several strategies have been evaluated, and the most common approaches include mechanical treatment, addition of chemical dispersants to the suspension, and chemical modification of the mineral surface.[28] Chemical treatments can modify the chemical properties of sepiolite and/or its toxicity in mammalian cells. Mechanical treatment can consist of ultrasound or high-speed shear processes, among others, which are capable of dispersing particle aggregates into smaller aggregates or simple particles without damaging the crystalline structure. Sonication has been presented as a relatively simple approach to disaggregate sepiolite fibers and improve their properties and characteristics.[26] Sonication involves the process of cavitation generation, which consists of the creation, growth, and collapse of bubbles formed in the liquid due to high intensity ultrasound irradiation.[31] In recent years, this technique has received much attention, especially due to the advent of nanotechnological applications for the assembly of nanoparticles to generate advanced functional nanoarchitectures, including sepiolite-based materials.[5,11] The sonication process makes it possible to improve the homogeneity of nanomaterials in suspensions and potentially achieve a smaller size distribution. In the field of nanomaterials and their application in biotechnology, the quality of the suspensions is very important, since this will determine the properties that can interfere with the nanomaterial interaction(s) with other molecules. This process can potentially alter the main physical and chemical properties of nanomaterials, such as size, morphology, increased contact surface area and surface charge distribution.[32,33] The literature has reported the importance of controlling the sonication process and the impact that it can have on the particle parameters.[34−38] More specifically, sonication of commercial sepiolite (Pangel S9) strongly stimulates the transfer of DNA into mammalian cells.[21] Therefore, it is essential to evaluate whether sonication affects the interaction of sepiolite with biological macromolecules and its potential detrimental effects on cell viability. In this respect, it is important to determine how different factors, such as power, duration, and temperature, can affect the quality of the dispersion. Although these considerations have been taken into account by some researchers, work in this area remains limited. Bihari et al. (2008) studied the stability of dispersions of different nanomaterials using different ultrasound energies with different dispersion stabilizers. Hartmann et al. (2015) highlighted that although work has been carried out to understand the different factors that affect the dispersion quality of nanomaterials, there is still no well-defined and universally accepted sonication procedure.

Here, we studied the process of deagglomeration/dispersion of sepiolite nanofibers to identify the optimum conditions for this process to produce detangled sepiolite for future biological applications. We first focused on the analysis of factors such as sonication time, sonicator power, temperature, and pH. Second, as a proof of concept, we analyzed the adsorption capacity of a protein (bovine serum albumin, BSA) and DNA on sonicated sepiolite (sSep). Finally, to assess whether sonication can affect sepiolite toxicity in mammalian cells, we analyzed the impact of the sonication of sepiolite on hemolytic activity in blood cells and toxicity/proliferation in human cell lines.

2. MATERIALS AND METHODS

2.1. Preparation of Sepiolite Suspension Using Vortex Dispersion. In this study, sepiolite (Sep) obtained from Vicálvaro-Vallecas deposits, Madrid (Spain), was generously supplied by TOLSA, S.A. with the trade name of Pangel S9. A 2 mg/mL sepiolite suspension was prepared in 10 mM Tris−HCl buffer, pH = 7.5, under vigorous vortexing at a maximum speed for a minimum time of 10 min to properly disperse the clay.

2.2. Preparation of Sepiolite Suspensions Using Ultrasound. Four tubes were prepared with sepiolite in 10 mL of a suspension in 10 mM Tris−HCl buffer, pH = 7.5, at a concentration of 2 mg/mL for ultrasonication. The clay was dispersed using a Vibra-Cell VC-50-1 (Sonics & Materials) with a standard Ti probe with a diameter and length of 13 mm and 138 mm, respectively, and a generator output power of 50 W. The sepiolite suspension was sonicated three times with an on/off pulse duration of 10 s at different sonication times (10, 20, 60, and 180 s). The procedure was repeated for each sonication time with amplitude settings of 30, 50, and 100%.

2.3. Effective Acoustic Power. The effective acoustic power delivered to the sonicated suspension is an important parameter for obtaining reproducible dispersions. This is different from the electrical input or output power of the generator indicated by the manufacturer as this is the actual power that is delivered to the suspension during sonication.[41] Among many methods for the calculation of effective delivered power, the most commonly used method is calorimetry.[41] This is known to be a simple and efficient way to directly measure the effective power delivered to a suspension.[42] In this method, the increase in temperature in the liquid at a given ultrasonic

https://doi.org/10.1021/acsomega.2c06391
ACS Omega 2023, 8, 1026−1036

equipment setting is recorded over time, and the effective power delivered is calculated using eq 1

$$P = \left(\frac{dT}{dt}\right)\cdot M\cdot C_p \quad (1)$$

where P is the delivered acoustic power, T is the temperature, t is the time, C_P is the specific heat of the liquid (4.18 $J.g^{-1}.K^{-1}$ for water), and M is the mass of the liquid.

2.4. Calorimetric Experiment. The temperature was measured using a digital thermometer (GESA Termómetros, S.L). The probe was introduced 4 cm below the surface of the liquid without touching the walls of the tube. The increase in temperature was recorded for 5 min at 30 s intervals. The data obtained allowed the construction of a temperature versus time graph; from this graph, the linear fit and the slope (which is the increase in temperature over time) were obtained. These data enable calculation of the effective acoustic power using eq 1. The experiment was repeated three times for each of the three amplitudes used.

2.5. Differential Centrifugation. The centrifugation study was performed for sSep solutions at different sonication times (10, 20, 60, and 180 s). Particles of different sizes in a suspension settle at different rates, and larger particles and denser sediment settle faster. By increasing the centrifugal force, the sedimentation rates can be increased. An Eppendorf 541712 centrifuge was used at varying angular velocity values of 0, 500, 1000, 2000, and 5000 rpm. Aliquots with a volume of 200 μL were taken at the mean height of the liquid in each sample, and the absorbance at a wavelength of 350 nm was measured using an Epoch Microplate spectrophotometer (BioTeK Instruments). The experiment was repeated three times for each sonication time.

2.6. Experimental Determination of the Sedimentation Velocity and the Aggregation Index. *2.6.1. Sedimentation Velocity.* The sedimentation velocity was determined using the data obtained for sedimentation of sepiolite suspensions with different sonication times. The samples were shaken so that they were as uniform as possible throughout the entire tube. Subsequently, the samples were left to rest, and the absorbance was measured at 0, 15, 30, and 60 min.

After determining the pairs of absorbance values as a function of time, the sedimentation curve was obtained. With this graphical representation, the sedimentation velocity was calculated as a function of the sonication time. From the experimental data obtained, the values for the slopes at the origin, ($dAbs/dt$), coincide with the sedimentation velocities.

2.6.2. Aggregation Index. The aggregation index (AI) was calculated using eq 2.[43,44]

$$AI = \left(\frac{OD_{Min}}{OD_{Max} - OD_{Min}}\right)\cdot 100 \quad (2)$$

where OD_{Max} represents the maximum in the absorbance band of the spectrum, OD_{Min} is the minimum absorbance; sepiolite shows light absorption predominantly at approximately 300−350 nm,.[45] The values for the max and min wavelengths were 350 and 600 nm, respectively.

2.7. sSep-Protein Synthesis. Protein solutions were prepared at different concentrations (5, 10, 20, 50, 100, 150, and 200 μg/mL). The protein used was bovine serum albumin (BSA): 2 mg/mL stock solutions were prepared in 10 mM Tris−HCl buffer, pH = 7.5. For each protein sample at different concentrations, 500 μL of sSep was added at a concentration of 100 μg/mL. The samples were completed with a 10 mM Tris−HCl, pH = 7.5 solution, until 1 mL was obtained for each sample. All sSep/protein mixtures were stirred overnight at 25 °C. Finally, the mixtures were centrifuged for 5 min at 5000 rpm, and the protein concentrations in the supernatants were measured using a NanoDrop ND1000 spectrophotometer.[39,40]

2.8. sSep− DNA Synthesis. For these samples, a Tris−HCl/$CaCl_2$ solution consisting of 25 mL of 20 mM Tris−HCl at pH = 7.5, 5 mL of 100 mM $CaCl_2$, and 20 mL of distilled water was prepared; 1 mL of sSep dispersion was taken at 2 mg/mL and centrifuged for 5 min at 5000 rpm, the supernatant was removed, and the precipitate was resuspended in 10 mL of Tris−HCl/$CaCl_2$ solution. Plasmid DNA was used, which was obtained by amplifying a bacterial culture and was purified using the NucleoBond Plasmid Purification Protocol. For each DNA sample at different concentrations, 500 μL of sSep in Tris−HCL/$CaCl_2$ was added at a concentration of 100 μg/mL. The samples were completed with 10 mM Tris−HCl, pH = 7.5 solution, until a volume of 1 mL was obtained for each sample. These samples were incubated under stirring overnight at 25 °C.

The mixtures were centrifuged for 5 min at 5000 rpm, and the DNA concentrations in the supernatants were measured using a NanoDrop ND1000 spectrophotometer.

2.9. Calculation of Adsorption Isotherms. To determine the adsorption isotherms for the different proteins used in our experiment, the concentration of the adsorbent phase was calculated using eq 3.[46]

$$q_e = \frac{(C_0 - C)\times V}{m} \quad (3)$$

where C_0 is the initial value of the protein concentrations (μg/mL), C is the protein concentration (μg/mL) in the supernatant, V denotes the volume (mL), and m (μg) is the amount of clay.

The adsorption performance was calculated, as shown in eq 4.[46,47]

$$\eta(\%) = \frac{(C_0 - C)}{C_0}\times 100 \quad (4)$$

2.10. Hemolytic Activity. Blood cells were extracted from human blood drawn from normal patients. The cells were washed three times with phosphate-buffered saline (PBS) solution. A suspension of erythrocytes was prepared by forming 2 mL of packed erythrocytes in 100 mL of PBS solution. A 0.1% sodium carbonate (Na_2CO_3) solution and a negative control PBS pH 7.4 were used as positive and negative controls, respectively.

For the evaluation of the compounds, 0.2 mL of erythrocyte solution was used, to which 10 μL of the sSep dispersion was added and brought to a volume of 10 mL with PBS. The positive control was evaluated by taking 0.2 mL of the erythrocyte solution and completing the 10 mL volume with 0.1% Na_2CO_3. For the negative control, 0.2 mL of erythrocyte solution was taken, and the volume was made up to 10 mL with PBS. Once the compound was added, the samples were carefully mixed and allowed to stand for 1 h at 37 °C.

The samples were centrifuged at 2000 rpm for 10 min. The absorbance at 545 nm was measured with a spectrophotometer (Pharmacia LKB·ULTROSPEC III).

https://doi.org/10.1021/acsomega.2c06391
ACS Omega 2023, 8, 1026−1036

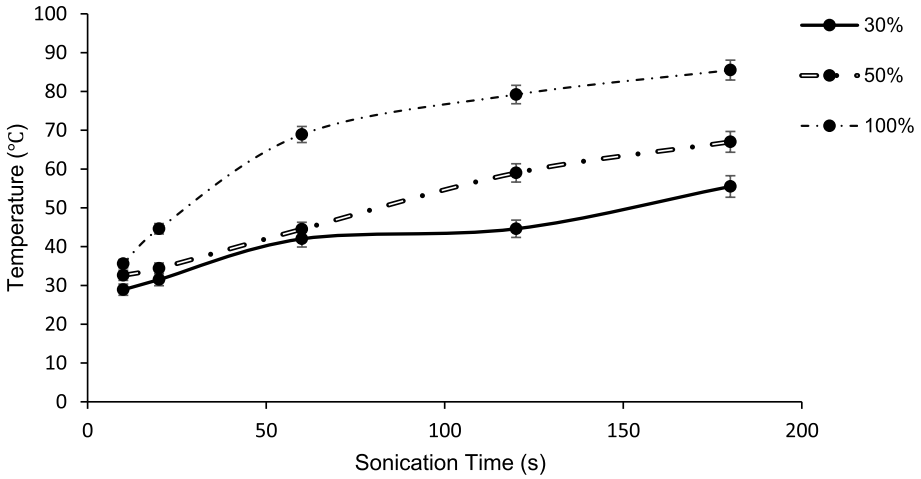

Figure 1. Calorimetric analysis with three different powers (%), as a function of the sonication times. Each point corresponds to three independent experiments (in triplicate for each repeat).

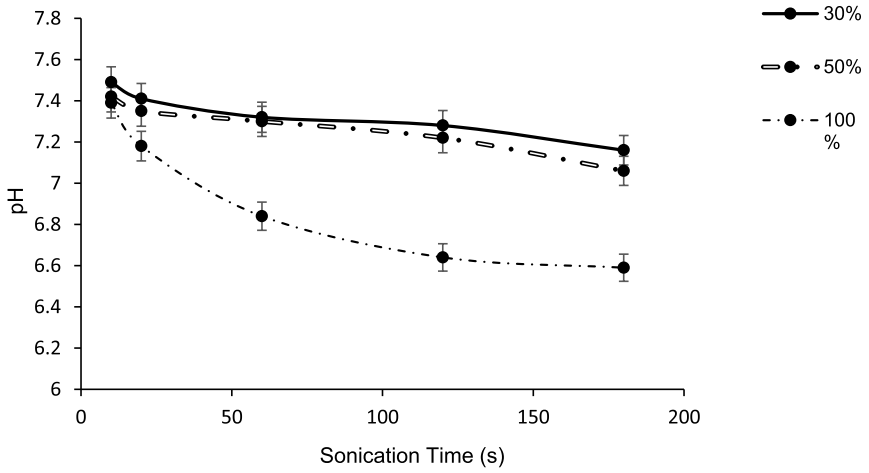

Figure 2. Analysis of pH as a function of sonication time for different input powers. Each point corresponds to three independent experiments (in triplicate for each repeat).

In each test, three replicates for each sSep dispersion and each reading were made. The hemolytic activity of sepiolite at different concentrations was calculated from the average absorbance for three repetitions and was expressed as a percentage using eq 5.[48]

$$\%H = \frac{OD_S \bullet OD_{NC}}{OD_{PC} \bullet OD_{NC}} \cdot 100 \quad (5)$$

where OD_S, OD_{NC}, and OD_{PC} are the optical density for the sample, negative control, and positive control, respectively.

2.11. Human Cell Toxicity Assay. The cell lines U2OS (human osteosarcoma) and RG37 (SV40-transformed human fibroblasts) were maintained at 37 °C with 5% CO_2 in modified Eagle's medium (MEM). One day after seeding of the cells, sepiolite (10 μg/mL) was added to the culture medium. Cells were collected 1 day after exposure to sepiolite. Cell pellets were resuspended in PBS and stained with the LIVE/DEAD Viability/Cytotoxicity Kit from Invitrogen (#L3224) according to the manufacturer's instructions. Flow cytometry analyses were performed using an Accuri C6 flow cytometer (BD Biosciences). A Calcein AM probe was used to measure the live cells (FL-1 channel), and an ethidium homodimer-1 probe was used to measure the dead cells (FL-2 channel).

2.12. AFM Imaging. Atomic force microscopy (AFM) imaging of sepiolite was performed using a freshly cleaved mica surface (V1 quality, EMS) treated with 50 μM spermidine for 1 min. Excess spermidine solution was blotted with a filter paper, and 3−5 μL of sepiolite dispersion was deposited onto the mica surface, incubated for 1−2 min, and rinsed with 25 μL of ultrapure water. The surface was blotted and dried. Imaging was carried out in the peak force mode with SCANASYST-Air probes (Bruker) with a Multimode system (Bruker) operating with a Nanoscope V controller (Bruker). All images were collected at a scan frequency of 1 Hz and a resolution of 1024 × 1024 pixels. Images were analyzed with Nanoscope V and ImageJ software. A third-order polynomial function was used to remove the background.

3. RESULTS AND DISCUSSION

3.1. Calorimetric Analysis. Although in principle, the increase of temperature produced by the treatment should not induce major transformation of the materials, we performed a calorimetric study. The calorimetric data reveal an increase in temperature with increasing sonication time (Figure 1). The

https://doi.org/10.1021/acsomega.2c06391
ACS Omega 2023, 8, 1026−1036

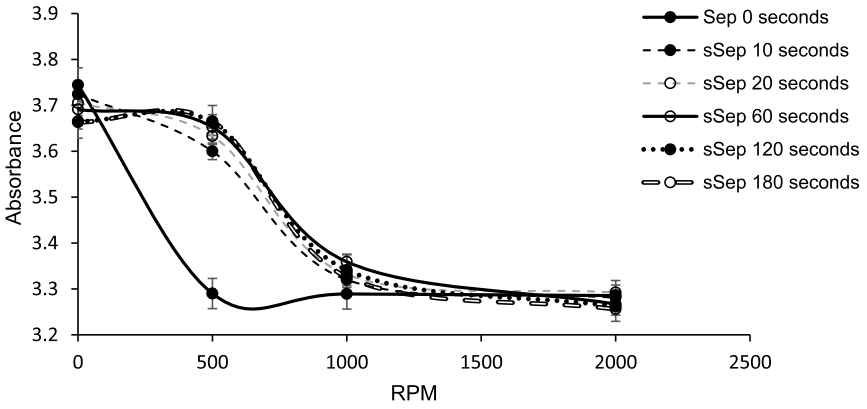

Figure 3. Centrifugation velocity of the sSep suspensions. Centrifugation was performed for 5 min for each speed indicated in the figure with different sonication times (indicated in the figure). Each point corresponds to three independent experiments (in triplicate for each repeat).

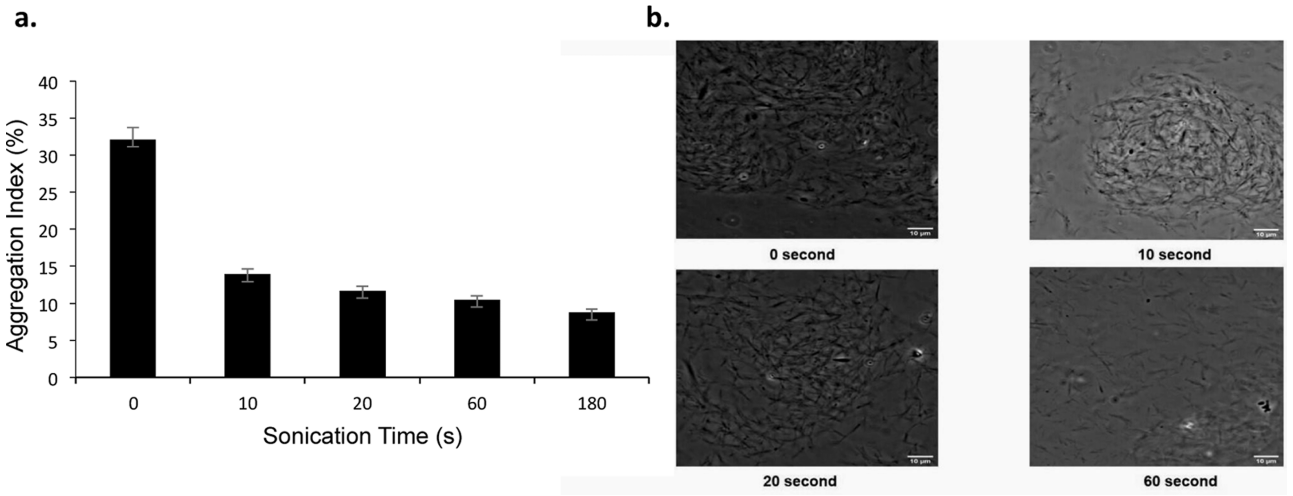

Figure 4. AI (a) and images of sepiolite nanofibers taken under a microscope (Leica Microsystems Microscope) (b). A standard transillumination technique of optical microscopy (bright field) was used, the dimensions of the images were 1024 × 1024, 16 bit per pixel and the objective 100×/1.45 (100× magnification and 1.45 numerical aperture). Data are taken from the average values for at least three independent experiments carried out in triplicate. Error bars represent the standard deviations. (b) Images of sepiolite nanofibers taken under a microscope (Leica Microsystems Fluorescence Microscope). Data are taken from the average values for at least three independent experiments carried out in triplicate. Error bars represent the standard deviations.

effective acoustic power delivered to the suspension at 30, 50, and 100% amplitude is 0.60 ± 0.02, 0.87 ± 0.03, and 1.18 ± 0.03 W, respectively.

The vibrational waves generated by ultrasound irradiation promote the creation of microbubbles, which undergo a process of expansion and collapse. This indicates that despite the high-energy source, most of the energy is lost during the generation of these microbubbles, and only a small fraction is actually delivered to the fibers in the suspension exposed to the ultrasound waves.[41,49]

Some studies have highlighted the importance of controlling the effective acoustic power compared to the input power of ultrasonic equipment for better control of dispersion during sonication.[49,50] In addition, the pH also evolves with sonication time and power. For the two lowest acoustic powers, a slight pH decrease is observed with increasing sonication time, while a stronger pH decrease with time is recorded for the highest power (Figure 2).

The lixiviation of magnesium from the clay can also affect the pH. One can suggest that with sonication and increasing sonication time, more magnesium can be lixiviated, resulting in a pH decrease. This can also affect the charge at the surface of the clay, which can be important in view of the interactions with the biomolecule.

As previously observed, there is a relationship between sonication time and temperature, but this parameter in turn can generate pH variations. Indeed, the temperature affects the pH since its variation is affected by the elements composing the solutions. An increase in temperature stimulates the dissociation of salts, acids, and bases, increasing the concentration of ions in the solution. In addition, increasing the temperature will decrease the viscosity and increase the mobility of the ions.

Since sepiolite absorbs biomolecules on its surface, it is important to consider the surface charge. The pH changes can lead to alterations in the surface charge of the fibers, leading to modifications in the adsorption of some ions.[51−53]

3.2. Dispersion of sSep. To estimate the dispersion efficiency, the sonicated nanoparticle solutions were subjected to centrifugation that enables separation of particles according to their mass. The absorbance in the UV−Vis range for the resulting supernatant is the most widely used method of detection for analytical centrifugation.[54]

https://doi.org/10.1021/acsomega.2c06391
ACS Omega 2023, 8, 1026−1036

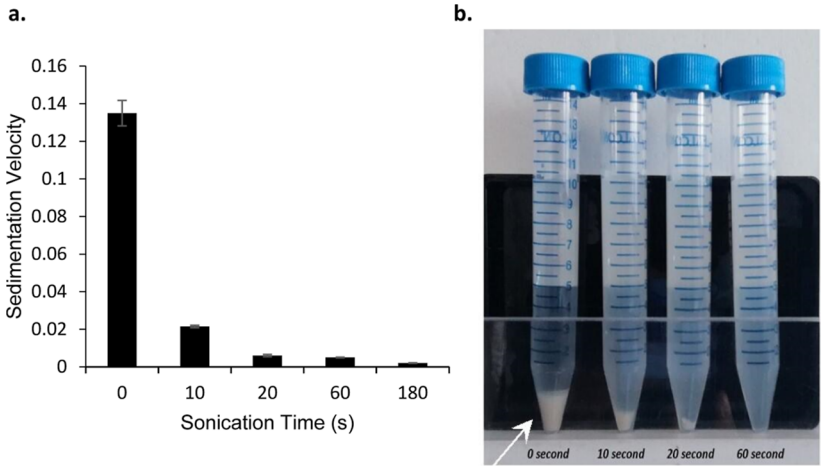

Figure 5. Sedimentation velocity (a) and 24 h of sedimentation of sepiolite sonicated for different times (indicated in the figure). The samples were left to rest, and the absorbance was measured at 0, 15, 30, and 60 min. The values correspond to the average of at least three independent experiments, each carried out in triplicate. Error bars represent the standard deviations. (b) Representative images after sedimentation of sSep. White arrow: sepiolite pellet.

Nonsonicated sepiolite samples were observed to reach centrifugation equilibrium at a speed lower than 500 rpm. This suggests that although the samples are defibrillated prior to sonication, they still contain aggregates and that the sizes of the aggregates or particles are large. In contrast, the sonicated samples reach centrifugation equilibrium at speeds higher than 1000 rpm (Figure 3), suggesting that the aggregates are smaller. No significant differences are observed for centrifugation speeds higher than 1000 rpm (Figure 3).

These data show that sonication leads to smaller aggregates/particles, even using Pangel S9, that is, corresponding to a previously detangled sepiolite sample. However, no differences are observed for varying sonication time. Therefore, to distinguish possible more subtle differences for different sonication times, we performed gentler analyses, and we measured the AI and the spontaneous sedimentation velocity. Indeed, the size of the particles also affects the sedimentation velocity, and the larger particles will precipitate at a higher velocity.

We analyzed the stability of the suspension and the aggregation by UV−Vis spectroscopy. Figure 4a shows the AI values obtained from analysis of the UV−Vis spectra and images obtained from fluorescence microscopy of the sonicated samples (Figure 4b).

The AI is predominantly affected by the particle size. The light scattering intensity increases with particle size, leading to greater AI values. Values below 10 usually represent solutions with insignificant amounts of soluble aggregates.[43] The data shown in Figure 4 show that nonsonicated sepiolite (defibrillated) still contains aggregates but that sonication dissociates these aggregates with an efficiency that increases with sonication time, with a strong effect obtained as soon as 10 s of sonication.

Then, we analyzed the impact of sonication on the spontaneous sedimentation of sepiolite fibers (Figure 5). Figure 5a shows the variation in sedimentation for the different sonication times. The different degrees of sedimentation should be noted (Figure 5b). A strong decrease is observed immediately after 10 s of sonication, which then progressively decreases with increasing sonication time (Figure 5a). Several theoretical and/or experimental studies have been carried out to evaluate the sedimentation process and to determine the sedimentation velocity of isolated particles and aggregates of particles settling in blocks. It has been found that there is an influence of shape, aggregation, and particle size on the sedimentation velocity of suspensions.[55,56] Here, the exposed sedimentation velocity data are consistent with the analysis of the AI (see above).

AFM images of sepiolite nanoclays have shown prominent size distribution and varied morphology.[30] The AFM analysis performed here (Figure 6) confirmed (i) the presence of aggregates in the nonsonicated initial sample of sepiolite and the dissociation of sepiolite aggregates upon sonication. Remarkably, a sonication time of 60 s leads to a shortening of the nanofiber length compared to that for a sonication time of 10 s (Figure 6).

62% of the sepiolite nanofibers are found to have a length ranging between 100 and 400 nm without ultrasonic treatment. This value does not change for sepiolite sonicated for 10 s (63%) but decreases to 44% for sepiolite sonicated for 60 s (Figure 6c).

The maximum lengths of the nonsonicated sepiolite are found to range from 1900−2000 nm for 0.75% of the nanofibers. With increasing sonication time, the range of maximum lengths decreases to 1800−1900 nm for 0.25% of the fibers, upon 10 s of sonication, and to [1600−1700] for 0.17% of the fibers upon 60 s of sonication. This shows a decrease in the maximum length with increasing sonication time. The proportion of nanofibers with lengths less than 100 nm is increased from 7 to 10% and 16% after treatment for 0, 10, and 60 s, respectively.

3.3. Impact of Sonication Time on the Adsorption of BSA and DNA. To assess whether the investigated sepiolite dispersion parameters impact the binding of biological macromolecules, we first measured the adsorption isotherms for sSep for two different kinds of essential biological molecules, that is, one model protein (bovine serum albumin, BSA) or DNA (Figure 7).

Remarkably, the two kinds of biological molecules behave differently. Indeed, while BSA protein adsorption increases with the dispersion of nanofibers (higher sonication time), DNA adsorption does not show significant difference with increasing sonication time (Figure 7).

https://doi.org/10.1021/acsomega.2c06391
ACS Omega 2023, 8, 1026−1036

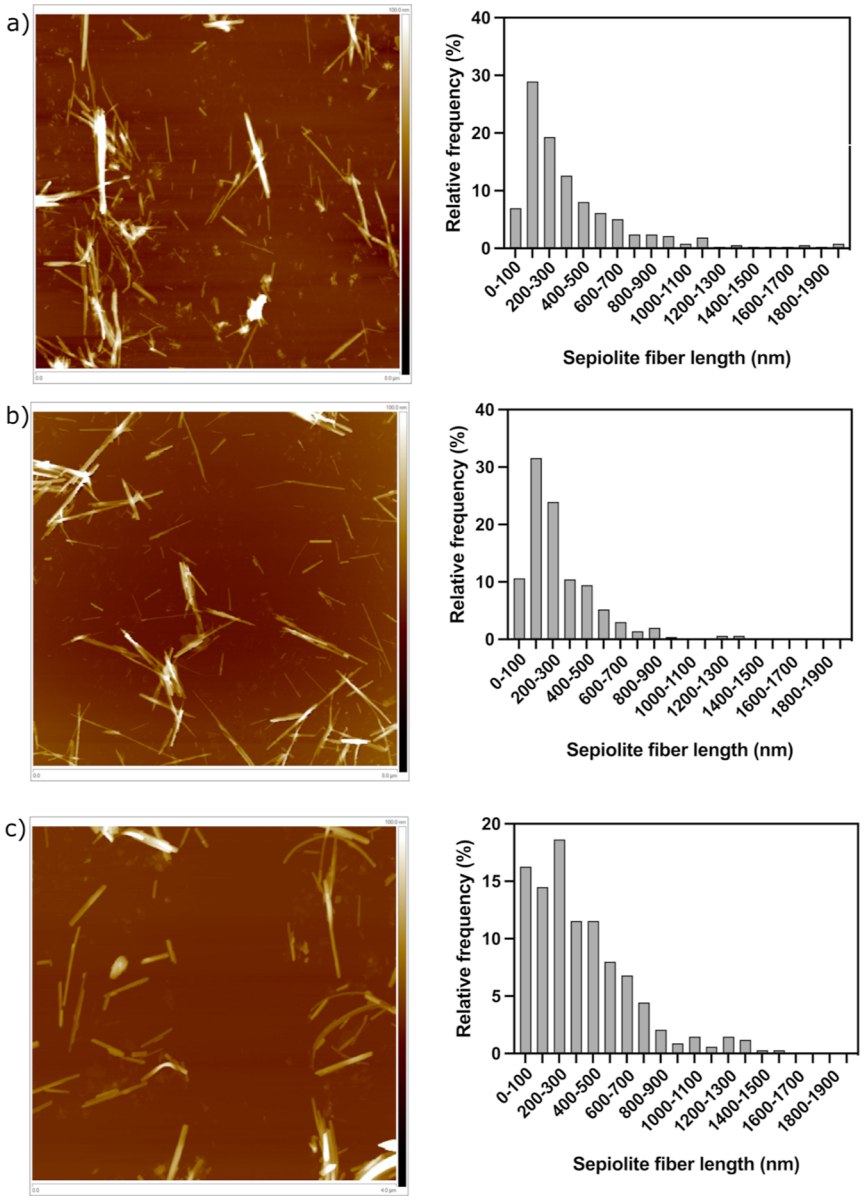

Figure 6. Sepiolite length distribution. Samples sonicated at (a) 0, (b) 10, and (c) 60; the insets show the AFM images for each distribution of sepiolite fibers [scan size 8 × 8 μm^2 for (a,b), and scan size 4 × 4 μm^2 for (c)]. Measurements were made on about 400 molecules for each experimental condition. The vertical scale bar is 100 nm.

Observations of the Sep/DNA bionanocomposites using TEM and AFM confirm that the DNA-sepiolite fiber assembly partially covers the surface of the sepiolite nanoparticles, and that, additionally, it is possible for more than two nanofibers to be linked by one DNA plasmid chain.[20] This aspect could be related to the low variation in DNA adsorption in relation to the sonication time.

3.4. Hemolytic Activity. To estimate the consequences of sepiolite sonication on human cells, we first monitored hemolytic (H) activity on erythrocytes, which reflects toxicity. Indeed, in the case where we would like to use sepiolite as a carrier for therapeutic molecules in future medical development, its impact on erythrocytes in blood becomes a paramount parameter, as discussed previously.[8,9,57] Interestingly, while nonsonicated sepiolite exhibits H values that range from approximately 80% (Figure 8), sonication of sepiolite decreases the H values as a function of sonication time. Notably, the H value drops to only 20% with sepiolite sonicated for 180 s (Figure 8). Some authors have reported changes in the hemolytic activity of sepiolite.[58,59] These changes are associated with the dimensions of the fibers, as well as the sources of the deposits, since this clay can contain impurities. Note that in our study, a shortening of the length of the nanofibers was observed.

These data suggest that sonication of sepiolite significantly reduces the toxicity of this mineral and that stronger treatment increases the dispersion of aggregates and reduces the fiber size, preventing sepiolite toxicity.

3.5. Impact of Sonication on Human Cell Toxicity. Hemolytic activity can be considered as a toxicity assay. However, erythrocytes are very specific cells, without a nucleus, and, thus, show limited metabolism; therefore, we analyzed the impact of sepiolite sonication on the toxicity of two different human cell lines: RG37 (a human SV40 transformed fibroblasts) and U2OS cells (from a human osteosarcoma). After 24 h of exposure, nonsonicated sepiolite

https://doi.org/10.1021/acsomega.2c06391
ACS Omega 2023, 8, 1026−1036

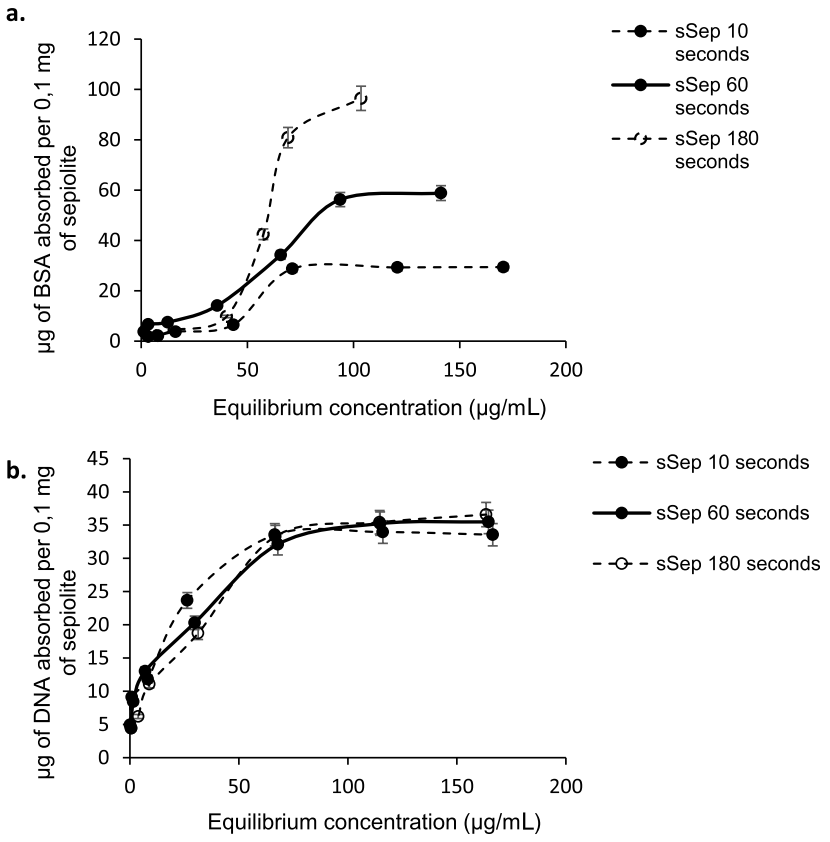

Figure 7. Adsorption isotherms for (a) BSA and (b) DNA on sepiolite. Each point has error bars for three different experiments carried out in triplicate for each condition. Reaction conditions: 10 mM Tris−HCl pH = 7.5 and a sepiolite concentration of 2 mg/mL. 100 μg of sepiolite was used in each experiment. Adsorption occurred at 25 °C under agitation overnight using a variable speed Thermo Scientific tube revolver/rotator.

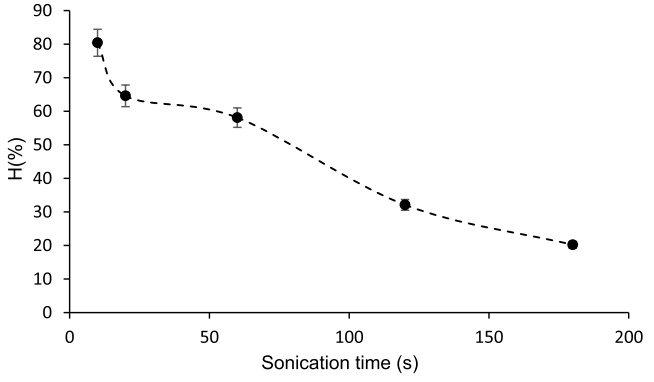

Figure 8. Hemolytic activity (H) of human red blood cells as a function of sonication time of sepiolite. Data show the average values taken from at least three independent experiments carried out in triplicate. Error bars represent the standard deviations.

increases the frequency of dead cells and, in parallel, decreases the frequency of living cells in both cell lines (Figure 9). Sonication of sepiolite rescues viability in both cell lines. Indeed, the frequency of dead cells drops, and in parallel, the frequency of living cells increases to levels close to that of untreated cells (Figure 9). However, the sonication time does not significantly influence the cell viability.

Collectively, the above reported data show that sonication of sepiolite decreases its toxicity. The fact that sonication time has no effect on the toxicity suggests that the toxicity predominantly results from the fiber aggregates rather than the size of the fibers (compare Figure 9 with Figure 6). These data might appear paradoxical because sonication should increase dispersion, and more cells should be affected. However, sepiolite fibers can be spontaneously internalized into cells but can also be spontaneously rejected from the cell, as we have previously shown.[21] The final toxicity depends on the final balance between these parameters. Indeed, toxicity depends on the equilibrium internalization/externalization from the cells; thanks to sonication, smaller aggregates should be more easily rejected, being thus less toxic, although more cells should be targeted. In contrast bigger aggregates should be less easily rejected and the fact that they are stuck in the cell leads to cell toxicity.

4. CONCLUSIONS

Here, we report that increasing the sepiolite sonication time enhances the adsorption efficiency for BSA, while this does not affect DNA binding efficiency. Finally, sonication of sepiolite diminishes both the hemolytic activity, and the cell proliferation decreases, suggesting that cell toxicity is decreased due to sonication of the sepiolite fibers.

The information presented throughout this work confirms the presence of aggregates in nonsonicated initial commercial samples of sepiolite but that their disaggregation is possible through sonication. Notably, a shortening of the nanofibers is observed for 3 × 60 s of ultrasonic treatment, compared to 3 × 10 s of treatment in the same experimental conditions. Increasing sonication time further might increase disaggregation and might shorten further the length of the fibers. Additionally, increased disaggregation might lead to the release of short fibers trapped in aggregates. However, it could be

https://doi.org/10.1021/acsomega.2c06391
ACS Omega 2023, 8, 1026−1036

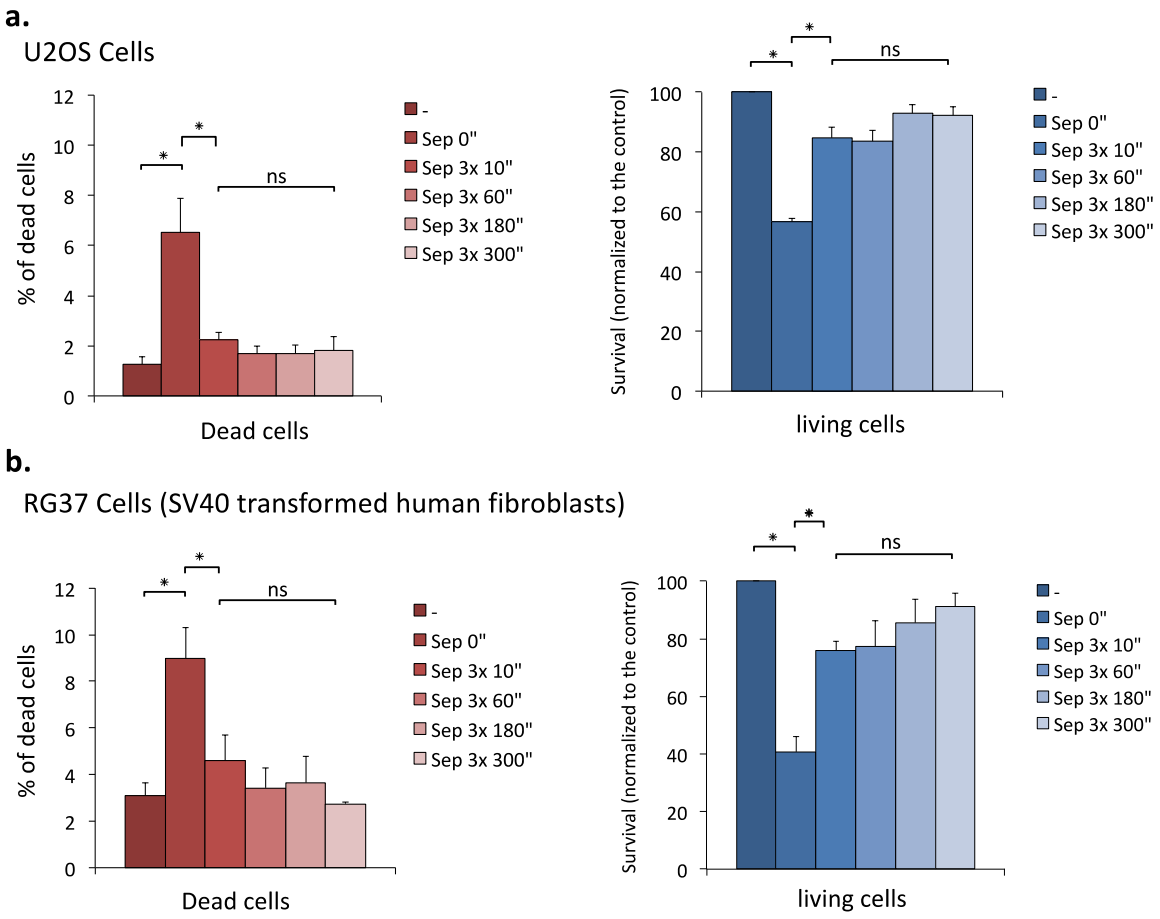

Figure 9. Toxicity of sepiolite in two different human cell lines. (a). U2OS cells. (b). RG37 human SV40-transformed fibroblasts. Red bars: frequency of dead cells; blue bars: frequency of living cells normalized to the untreated cells. The sonication times are indicated in the figures. The values shown correspond to the mean values from three independent experiments. Statistics; Mann–Whitney tests; *: $p < 0.05$; ns; not significant. GraphPad Prism software was used for statistical analysis.

expected that a plateau level could be reached for long sonication times. Remarkably, sonication of the sepiolite samples used here does not impact the efficiency of DNA binding but improves the efficiency of binding of one model protein, BSA, and, importantly, decreases the toxicity in mammalian cells. We cannot exclude that further increase of sonication time might allow to reach a threshold above which the DNA binding would be improved. Possibly, the binding of proteins might be improved, and the cell toxicity further decreased. However, plateau levels might also be reached for these parameters. Note that our data suggest that sepiolite microfibril aggregation could result in cell toxicity. Therefore, commercially available sepiolite (Pangel S9), supplied as a partially defibrillated clay mineral, could still be significantly improved by sonication, especially useful for future biomedical applications. The fact that ultrasonication improves the binding of biological macromolecules (such as proteins) and, in parallel, reduces the cell toxicity, might represent a very alluring improvement to use sepiolite in some biomedical applications, such as non-viral vector for cancer treatment.

AUTHOR INFORMATION

Corresponding Author

Bernard S. Lopez − *Université de Paris Cité, INSERM U1016, UMR 8104 CNRS, Institut Cochin, Equipe Labellisée Ligue Contre le Cancer, Paris 75014, France;* orcid.org/0000-0001-5088-0155; Email: bernard.lopez@inserm.fr

Authors

David Adame Brooks − *Université de Paris Cité, INSERM U1016, UMR 8104 CNRS, Institut Cochin, Equipe Labellisée Ligue Contre le Cancer, Paris 75014, France; Centro de Biofísica Médica, Universidad de Oriente, Santiago de Cuba CP 90500, Cuba*

Olivier Piétrement − *Laboratoire Interdisciplinaire Carnot de Bourgogne, CNRS UMR 6303, Université de Bourgogne-Franche-Comté, Dijon Cedex 21078, France;* orcid.org/0000-0002-0018-7202

Elodie Dardillac − *Université de Paris Cité, INSERM U1016, UMR 8104 CNRS, Institut Cochin, Equipe Labellisée Ligue Contre le Cancer, Paris 75014, France*

Ayesha Jayantha − *Laboratoire Interdisciplinaire Carnot de Bourgogne, CNRS UMR 6303, Université de Bourgogne-Franche-Comté, Dijon Cedex 21078, France*

Manuel A. Lores Guevara − *Centro de Biofísica Médica, Universidad de Oriente, Santiago de Cuba CP 90500, Cuba*

Fidel Antonio Castro-Smirnov − *Universidad de las Ciencias Informáticas, La Habana 19370, Cuba*

Pilar Aranda − *Instituto de Ciencia de Materiales de Madrid, CSIC, Madrid 28049, Spain*

https://doi.org/10.1021/acsomega.2c06391
ACS Omega 2023, 8, 1026−1036

Eduardo Ruiz-Hitzky − *Instituto de Ciencia de Materiales de Madrid, CSIC, Madrid 28049, Spain;* orcid.org/0000-0003-4383-7698

Complete contact information is available at: https://pubs.acs.org/10.1021/acsomega.2c06391

Author Contributions

D.A.B. performed physicochemical characterization and hemolytic activity. E.D. performed toxicity experiments in human cell lines. O.P. and A.J. performed AFM experiments. D.A.B., O.P., E.D., P.A., and E.R.H. interpreted the data. D.A.B. and B.S.L. conceived the experiments. B.S.L. supervised the project. All authors discussed the results and commented on the manuscript. The manuscript was written through contributions of all authors. All authors have given approval to the final version of the manuscript.

Notes

The authors declare no competing financial interest.

■ ACKNOWLEDGMENTS

We thank Ivan Matic's laboratory (Institut Cochin) for helpful technical assistance for fluorescence microscopy. This work is supported by grants from the Ligue Nationale contre le cancer "Equipe labellisée 2017", ITMO Cancer (PCSI 2022), and INCa (Institut National du Cancer 2018-1-PLBIO-07) (B.S.L.). D.A.B. and F.A.C.S. were supported by financial support from the French Embassy in Cuba. O.P. and A.J. were supported by funding from the CNRS Mission pour l'Interdisciplinarité (MI-DynAFM-DNARep 2018_273085), région Bourgogne-Franche-Comté (AAP Région 2020—ANER—Projet AFMdynDNA, AAP Région 2020 DNA-Heritage), and the EIPHI Graduate School (contract ANR-17-EURE-0002). P.A. and E.R.H. acknowledge support from MCIN/AEI/10.13039/501100011033 (Spain, project PID2019-105479RB-100).

■ ABBREVIATIONS

sSep, sonicated sepiolite; AFM, atomic force microscopy; BSA, bovine serum albumin; AI, aggregation index

■ REFERENCES

(1) Suárez, M.; García-Romero, E.Advances in the Crystal Chemistry of Sepiolite and Palygorskite*The Netherlands Developments in Clay Science*, Galan, E., Singer, A., Eds.; Elsevier, 2011; Vol. 3, pp 33−65: Amsterdam

(2) Brigatti, M. F.; Galán, E.; Theng, B. K. G. Structure and Mineralogy of Clay Minerals. *Dev. Clay Sci.* **2013**, *5*, 21−81.

(3) Rodríguez-Beltrán, J.; Rodríguez-Rojas, A.; Yubero, E.; Blázquez, J. The Animal Food Supplement Sepiolite Promotes a Direct Horizontal Transfer of Antibiotic Resistance Plasmids between Bacterial Species. *Antimicrob. Agents Chemother.* **2013**, *57*, 2651−2653.

(4) Zayed, M. A.; El-Begawy, S. E. M.; Hassan, H. E. S. Enhancement of Stabilizing Properties of Double-Base Propellants Using Nano-Scale Inorganic Compounds. *J. Hazard. Mater.* **2012**, *227−228*, 274−279.

(5) Ruiz-Hitzky, E.; Aranda, P.; Álvarez, A.; Santarén, J.; Esteban-Cubillo, A.Advanced Materials and New Applications of Sepiolite and Palygorskite*Developments in Palygorskite-Sepiolite Research. A New Outlook on These Nanomaterials*Galan, E., Singer, A., Eds.; Elsevier: Oxford, 2011; Vol. 3, pp 393−452.

(6) Alcântara, A. C. S.; Darder, M.; Aranda, P.; Ayral, A.; Ruiz-Hitzky, E. Bionanocomposites Based on Polysaccharides and Fibrous Clays for Packaging Applications. *J. Appl. Polym. Sci.* **2016**, *133*, 1.

(7) Ruiz-Hitzky, E.; Sobral, M. M. C.; Gómez-Avilés, A.; Nunes, C.; Ruiz-García, C.; Ferreira, P.; Aranda, P. Clay-Graphene Nanoplatelets Functional Conducting Composites. *Adv. Funct. Mater.* **2016**, *26*, 7394−7405.

(8) Piétrement, O.; Castro-Smirnov, F. A.; Le Cam, E.; Aranda, P.; Ruiz-Hitzky, E.; Lopez, B. S. Sepiolite as a New Nanocarrier for DNA Transfer into Mammalian Cells: Proof of Concept, Issues and Perspectives. *Chem. Rec.* **2018**, *18*, 849−857.

(9) Castro-Smirnov, F. A.; Piétrement, O.; Aranda, P.; Le Cam, E.; Ruiz-Hitzky, E.; Lopez, B. S. Biotechnological Applications of the Sepiolite Interactions with Bacteria: Bacterial Transformation and DNA Extraction. *Appl. Clay Sci.* **2020**, *191*, 105613.

(10) Ragu, S.; Piétrement, O.; Lopez, B. S. Binding of DNA to Natural Sepiolite: Applications in Biotechnology and Perspectives. *Clays Clay Miner.* **2021**, *69*, 633.

(11) Aranda, P.; Ruiz-Hitzky, E. Immobilization of Nanoparticles on Fibrous Clay Surfaces: Towards Promising Nanoplatforms for Advanced Functional Applications. *Chem. Rec.* **2018**, *18*, 1125−1137.

(12) Rajczak, E.; Arrigo, R.; Malucelli, G. Thermal Stability and Flame Retardance of EVA Containing DNA-Modified Clays. *Thermochim. Acta* **2020**, *686*, 178546.

(13) Peixoto, D.; Pereira, I.; Pereira-Silva, M.; Veiga, F.; Hamblin, M. R.; Lvov, Y.; Liu, M.; Paiva-Santos, A. C. Emerging Role of Nanoclays in Cancer Research, Diagnosis, and Therapy. *Coord. Chem. Rev.* **2021**, *440*, 213956.

(14) Wang, Z.; Liao, L.; Hursthouse, A.; Song, N.; Ren, B. Sepiolite-Based Adsorbents for the Removal of Potentially Toxic Elements from Water: A Strategic Review for the Case of Environmental Contamination in Hunan, China. *Int. J. Environ. Res. Public Health* **2018**, *15*, 1653.

(15) Dabiri, R.; Amiri Shiraz, E. Evaluating Performance of Natural Sepiolite and Zeolite Nanoparticles for Nickel, Antimony, and Arsenic Removal from Synthetic Wastewater. *J. Min. Environ.* **2018**, *9*, 1049−1064.

(16) Xie, S.; Zhang, S.; Wang, F.; Yang, M.; Séguéla, R.; Lefebvre, J. M. Preparation, Structure and Thermomechanical Properties of Nylon-6 Nanocomposites with Lamella-Type and Fiber-Type Sepiolite. *Compos. Sci. Technol.* **2007**, *67*, 2334−2341.

(17) Lo Dico, G.; Wicklein, B.; Lisuzzo, L.; Lazzara, G.; Aranda, P.; Ruiz-Hitzky, E. Multicomponent Bionanocomposites Based on Clay Nanoarchitectures for Electrochemical Devices. *Beilstein J. Nanotechnol.* **2019**, *10*, 1303−1315.

(18) González del Campo, M. M.; Darder, M.; Aranda, P.; Akkari, M.; Huttel, Y.; Mayoral, A.; Bettini, J.; Ruiz-Hitzky, E. Functional Hybrid Nanopaper by Assembling Nanofibers of Cellulose and Sepiolite. *Adv. Funct. Mater.* **2018**, *28*, 1703048−13.

(19) Ruiz-Hitzky, E.; Darder, M.; Fernandes, F. M.; Wicklein, B.; Alcântara, A. C. S.; Aranda, P. Fibrous Clays Based Bionanocomposites. *Prog. Polym. Sci.* **2013**, *38*, 1392−1414.

(20) Castro-Smirnov, F. A.; Piétrement, O.; Aranda, P.; Bertrand, J.-R. J.-R.; Ayache, J.; Le Cam, E.; Ruiz-Hitzky, E.; Lopez, B. S. Physical Interactions between DNA and Sepiolite Nanofibers, and Potential Application for DNA Transfer into Mammalian Cells. *Sci. Rep.* **2016**, *6*, 36341.

(21) Castro-Smirnov, F. A.; Ayache, J.; Bertrand, J.-R. J.-R.; Dardillac, E.; Le Cam, E.; Piétrement, O.; Aranda, P.; Ruiz-Hitzky, E.; Lopez, B. S. Cellular Uptake Pathways of Sepiolite Nanofibers and DNA Transfection Improvement. *Sci. Rep.* **2017**, *7*, 5586.

(22) Alcântara, A. C. S.; Darder, M.; Aranda, P.; Ruiz-Hitzky, E. Polysaccharide−Fibrous Clay Bionanocomposites. *Appl. Clay Sci.* **2014**, *96*, 2−8.

(23) Ruiz-Hitzky, E.; Darder, M.; Wicklein, B.; Fernandes, F. M.; Castro-Smirnov, F. A.; Martín del Burgo, M. A.; del Real, G.; Aranda, P. Advanced Biohybrid Materials Based on Nanoclays for Biomedical Applications. *Proc. SPIE* **2012**, *8548*, 85480D.

(24) Wicklein, B.; Darder, M.; Aranda, P.; Ruiz-Hitzky, E. Bio-Organoclays Based on Phospholipids as Immobilization Hosts for Biological Species. *Langmuir* **2010**, *26*, 5217−5225.

(25) Ruiz-Hitzky, E. Molecular Access to Intracrystalline Tunnels of Sepiolite. *J. Mater. Chem.* **2001**, *11*, 86−91.
(26) Ruiz-Hitzky, E.; Ruiz-García, C.; Fernandes, F. M.; Lo Dico, G.; Lisuzzo, L.; Prevot, V.; Darder, M.; Aranda, P. Sepiolite-Hydrogels: Synthesis by Ultrasound Irradiation and Their Use for the Preparation of Functional Clay-Based Nanoarchitectured Materials. *Front. Chem.* **2021**, *9*, 1−17.
(27) Berenguer, A.; Perez Castells, R.; Aragon Martinez, J. J.; Esteban Aldezabal, M. A.*A Rheological Grade Sepiolite Product and Processes for Its Manufacture*; European patent application, EP0170299, 1985.
(28) Alves, L.; Ferraz, E.; Santarén, J.; Rasteiro, M. G.; Gamelas, J. A. F. Improving Colloidal Stability of Sepiolite Suspensions: Effect of the Mechanical Disperser and Chemical Dispersant. *Minerals* **2020**, *10*, 779−20.
(29) Wang, A.; Wang, W.*Introduction. In Nanomaterials from Clay Minerals*; Aiqin Wang, W. W., Ed.; Elsevier: Amsterdam, 2019, pp 1−20.
(30) Iakovlev, I. A.; Deviatov, A. Y.; Lvov, Y.; Fakhrullina, G.; Fakhrullin, R. F.; Mazurenko, V. V. Probing Diffusive Dynamics of Natural Tubule Nanoclays with Machine Learning. *ACS Nano* **2022**, *16*, 5867−5873.
(31) Yin, L.; Wang, Y.; Pang, G.; Koltypin, Y.; Gedanken, A. Sonochemical Synthesis of Cerium Oxide Nanoparticles - Effect of Additives and Quantum Size Effect. *J. Colloid Interface Sci.* **2002**, *246*, 78−84.
(32) Mandzy, N.; Grulke, E.; Druffel, T. Breakage of TiO2 Agglomerates in Electrostatically Stabilized Aqueous Dispersions. *Powder Technol.* **2005**, *160*, 121−126.
(33) Farré, M.; Gajda-Schrantz, K.; Kantiani, L.; Barceló, D. Ecotoxicity and Analysis of Nanomaterials in the Aquatic Environment. *Anal. Bioanal. Chem.* **2009**, *393*, 81−95.
(34) Jiang, J.; Oberdörster, G.; Biswas, P. Characterization of Size, Surface Charge, and Agglomeration State of Nanoparticle Dispersions for Toxicological Studies. *J. Nanoparticle Res.* **2009**, *11*, 77−89.
(35) Wu, W.; Ichihara, G.; Suzuki, Y.; Izuoka, K.; Oikawa-tada, S.; Chang, J.; Sakai, K.; Miyazawa, K.; Porter, D.; Castranova, V.; Kawaguchi, M.; Ichihara, S. Dispersion Method for Safety Research on Manufactured Nanomaterials. *Ind. Health* **2014**, *52*, 54−65.
(36) Meißner, T.; Oelschlägel, K.; Potthoff, A. Dispersion of Nanomaterials Used in Toxicological Studies: A Comparison of Sonication Approaches Demonstrated on TiO2 P25. *J. Nanoparticle Res.* **2014**, *16*, 2228.
(37) Cronholm, P.; Midander, K.; Karlsson, H. L.; Elihn, K.; Wallinder, I. O.; Möller, L. Effect of Sonication and Serum Proteins on Copper Release from Copper Nanoparticles and the Toxicity towards Lung Epithelial Cells. *Nanotoxicology* **2011**, *5*, 269−281.
(38) Murdock, R. C.; Braydich-Stolle, L.; Schrand, A. M.; Schlager, J. J.; Hussain, S. M. Characterization of Nanomaterial Dispersion in Solution Prior to in Vitro Exposure Using Dynamic Light Scattering Technique. *Toxicol. Sci.* **2008**, *101*, 239−253.
(39) Bihari, P.; Vippola, M.; Schultes, S.; Praetner, M.; Khandoga, A. G.; Reichel, C. A.; Coester, C.; Tuomi, T.; Rehberg, M.; Krombach, F. Optimized Dispersion of Nanoparticles for Biological in Vitro and in Vivo Studies. *Part. Fibre Toxicol* **2008**, *5*, 14.
(40) Hartmann, N. B.; Jensen, K. A.; Baun, A.; Rasmussen, K.; Rauscher, H.; Tantra, R.; Cupi, D.; Gilliland, D.; Pianella, F.; Riego Sintes, J. M. Techniques and Protocols for Dispersing Nanoparticle Powders in Aqueous Media - Is There a Rationale for Harmonization? *J. Toxicol. Environ. Heal. - Part B Crit. Rev.* **2015**, *18*, 299−326.
(41) Yamaguchi, K. I.; Matsumoto, T.; Kuwata, K. Proper Calibration of Ultrasonic Power Enabled the Quantitative Analysis of the Ultrasonication-Induced Amyloid Formation Process. *Protein Sci.* **2012**, *21*, 38−49.
(42) Taurozzi, J. S.; Hackley, V. A.; Wiesner, M. R. Ultrasonic Dispersion of Nanoparticles for Environmental, Health and Safety Assessment Issues and Recommendations. *Nanotoxicology* **2011**, *5*, 711−729.
(43) Katayama, D. S.; Nayar, R.; Chou, D. K.; Campos, J.; Cooper, J.; Vander Velde, D. G.; Villarete, L.; Liu, C. P.; Cornell Manning, M. C. Solution behavior of a novel type 1 interferon, interferon-τ. *J. Pharm. Sci.* **2005**, *94*, 2703−2715.
(44) Hawe, A.; Kasper, J. C.; Friess, W.; Jiskoot, W. Structural Properties of Monoclonal Antibody Aggregates Induced by Freeze-Thawing and Thermal Stress. *Eur. J. Pharm. Sci.* **2009**, *38*, 79−87.
(45) Chuaicham, C.; Pawar, R.; Sasaki, K. Dye-Sensitized Photocatalyst of Sepiolite for Organic Dye Degradation. *Catalysts* **2019**, *9*, 235.
(46) Olalekan, A.; Olatunya, A.; Dada, O. Langmuir, Freundlich, Temkin and Dubinin−Radushkevich Isotherms Studies of Equilibrium Sorption of Zn 2+ Unto Phosphoric Acid Modified Rice Husk. *IOSR J. Appl. Chem.* **2012**, *3*, 38−45.
(47) Kopac, T.; Bozgeyik, K.; Flahaut, E. Adsorption and Interactions of the Bovine Serum Albumin-Double Walled Carbon Nanotube System. *J. Mol. Liq.* **2018**, *252*, 1−8.
(48) Alonso Geli, Y.; Del Toro García, G.; Falcón Dieguez, J. E.; Valdés Rodríguez, Y. C. Actividad Hemolítica de La Ortovainillina y La Isovainillina Sobre Eritrocitos Humanos. *Rev. Cuba. Farm.* **2005**, *39*, 1561.
(49) Kaur, I.; Ellis, L. J.; Romer, I.; Tantra, R.; Carriere, M.; Allard, S.; Mayne-L'Hermite, M.; Minelli, C.; Unger, W.; Potthoff, A.; Rades, S.; Valsami-Jones, E. Dispersion of Nanomaterials in Aqueous Media: Towards Protocol Optimization. *J. Vis. Exp.* **2017**, *2017*, 56074.
(50) Sesis, A.; Hodnett, M.; Memoli, G.; Wain, A. J.; Jurewicz, I.; Dalton, A. B.; Carey, J. D.; Hinds, G. Influence of Acoustic Cavitation on the Controlled Ultrasonic Dispersion of Carbon Nanotubes. *J. Phys. Chem. B* **2013**, *117*, 15141−15150.
(51) Ozdemir, O.; Cinar, M.; Sabah, E.; Arslan, F.; Celik, M. S. Adsorption of Anionic Surfactants onto Sepiolite. *J. Hazard. Mater.* **2007**, *147*, 625−632.
(52) Alkan, M.; Demirbaş, Ö.; Doğan, M. Electrokinetic Properties of Sepiolite Suspensions in Different Electrolyte Media. *J. Colloid Interface Sci.* **2005**, *281*, 240−248.
(53) Lazarević, S.; Janković-Častvan, I.; Jovanović, D.; Milonjić, S.; Janaćković, D.; Petrović, R. Adsorption of Pb2+, Cd2+ and Sr2+ Ions onto Natural and Acid-Activated Sepiolites. *Appl. Clay Sci.* **2007**, *37*, 47−57.
(54) Cole, J. L.; Lary, J. W.; Moody, P.; Laue, T. M. Analytical Ultracentrifugation: Sedimentation Velocity and Sedimentation Equilibrium. *Methods Cell Biol* **2008**, *84*, 143−179.
(55) COMINI, B. C.; ZEGARRA, J. L. Determinación Experimental de La Velocidad de Caída de Sedimentos No Cohesivos. *Ingeniare. Rev. Chil. Ing.* **2020**, *28*, 236−247.
(56) Bargieł, M.; Tory, E. M. Extension of the Richardson-Zaki Equation to Suspensions of Multisized Irregular Particles. *Int. J. Miner. Process.* **2013**, *120*, 22−25.
(57) Ragu, S.; Dardillac, E.; Brooks, D.; Castro-Smirnov, F. A.; Aranda, P.; Ruiz-Hitzky, E.; Lopez, B. S. Responses of Human Cells to Sepiolite Interaction. *Appl. Clay Sci.* **2020**, *194*, 105655.
(58) Koshi, K.; Kohyama, N.; Myojo, T.; Fukuda, K. Cell Toxicity, Hemolytic Action and Clastogenic Activity of Asbestos and Its Substitutes. *Ind Heal* **1991**, *29*, 37−56.
(59) Hayashi, H. Occurrences and Biological Effects of Sepiolite and Palygorskite. *J. Soc. Mater. Eng. Resour. Japan* **1995**, *8*, 99−112.

https://doi.org/10.1021/acsomega.2c06391
ACS Omega 2023, 8, 1026−1036